Axial Heterostructures with Phase-Controlled Metastable Segments via Post-Growth Reactions of Ge Nanowires

Eli Sutter[1] *and Peter Sutter*[2,]*

[1]Department of Mechanical and Materials Engineering, University of Nebraska-Lincoln, Lincoln, NE 68588 (USA), [2]Department of Electrical and Computer Engineering, University of Nebraska-Lincoln, Lincoln, NE 68588 (USA)

*Corresponding author, e-mail: psutter@unl.edu

Abstract

Metastable crystal phases promise new functionalities by providing access to materials properties beyond those of thermodynamically stable crystalline solids. While realizing metastable phases in the bulk requires non-equilibrium processes such as rapid quenching or high pressures, size effects at the nanometer scale can promote their formation and stabilization during mild processing. Here we demonstrate the controlled formation of axial heterostructures of alternating stable semiconductor (Ge) and metastable metallic (AuGe) segments *via* post-growth processing, by decorating Ge nanowires with Au, encapsulating them in graphitic carbon shells, annealing at moderate temperatures to induce alloying of Au and Ge in the melt, followed by slow cooling and crystallization. The process is extended to form heterostructures of binary AgGe and ternary AuAgGe alloy segments in Ge nanowires. The metallic alloys adopt different metastable crystal phases that are selected *via* the nanowire diameter. This phase selection, explained by a size-dependent solubility of Ge in liquid AuGe (and AgGe) and distinct structural motifs in Ge-rich AuGe melts, allows establishing a previously unknown metastable γ-AgGe metastable in thin axially segmented Ge-AgGe nanowires. The findings demonstrate an avenue for synthesizing axial heterostructures of stable and metastable solid phases in nanowires.

1. Introduction

Hybrid nanostructures that incorporate junctions between dissimilar materials, such as semiconductors and metals, are promising for applications in photocatalysis,[1-3] plasmonics,[4] electronic devices,[5] nano-bioelectronics and sensors,[6,7] solar cells,[8] *etc.* Nanowires support two types of heterojunctions, radial and axial. Radial (core-shell) nanowire heterostructures have been investigated for solar-to-fuel conversion,[9] electronics,[10] electrocatalysis (metal-metal),[11] and photocatalysis (semiconductor-semiconductor),[12] while axially segmented nanowire heterostructures have been considered for high-performance electrocatalysis, nanomotors (metal-metal),[13] or for applications requiring control over magnetic domain walls.[14] Axially segmented semiconductor-semiconductor and metal-semiconductor[15] nanowires have been fabricated *via* sequential vapor-liquid-solid (VLS) growth,[16-20] as well as alternative approaches such as post-growth oxidation[21] or anodic alumina templated electrochemical deposition.[6,22] Orru *et al.* demonstrated the formation of Au-rich metallic segments by thermally activated diffusion from metal contacts into GaAs nanowires.[5]

The incorporation of metastable crystal phases is a possible strategy toward creating nanowire heterostructures with new functionalities from an expanded set of crystalline materials. Au-Ge and Ag-Ge are metallic systems of interest for integration with semiconductors in nanowires[22] and other types of metal-semiconductor junctions at the nanoscale.[23,24] Binary AuGe and AgGe alloys both have eutectic-type phase diagrams with relatively low eutectic temperatures (361°C and 650°C, respectively) and similar eutectic compositions (27 at.% and 25.9 at.% Ge, respectively),[25-27] which make them suitable as catalyst melt drops for VLS nanowire growth. Indeed, the VLS growth of Ge nanowires typically involves Au catalyst nanoparticles, which convert into AuGe alloy melts during Ge deposition.[28-30] Au-Ag alloy nanoparticles have also been used as VLS catalysts as they allow for higher supersaturations and thus achieve smaller Ge nanowire diameters.[31]

In the bulk, metastable crystalline AuGe and AgGe phases can be obtained when alloys close

to (or more-Ge rich than) the eutectic compositions are rapidly quenched from the melt,[25,32-34] or by applying high pressures.[25,35] In this way, bulk alloys close to eutectic composition can crystallize as metastable hexagonal close-packed (hcp) β-Au-(20 at.%) Ge[25,32,34,35] and β–Ag-(26 at.%) Ge,[25,36] respectively. Bulk Au-Ge alloys with higher Ge content (40-50 at.%) have been reported to crystallize in a second metastable phase, body centered tetragonal (bct) γ-AuGe.[32] No such second phase has been observed for bulk AgGe alloys.[32,34] In Ge nanowires grown by the VLS process with Au nanoparticle seeds, the metastable β-AuGe phase is occasionally observed in the Au-rich nanowire tips after growth.[37-40] Segmented nanowires of alternating metastable metallic β-AuGe and semiconducting Ge have been grown in porous anodic alumina templates, albeit limited to relatively large diameters (≳80 nm), defined by the size of the pores. Isolation of the axial nanowires required etching of the template.[22] We previously demonstrated the possibility of forming single segments of the two different metastable Au-Ge phases, β-AuGe and γ-AuGe, at the tips of Ge nanowires using annealing to elevated temperatures.[40,41]

Here we use variable-temperature *in-situ* transmission electron microscopy (TEM) to demonstrate an approach toward axial nanowire heterostructures of alternating Ge and metastable AuGe segments *via* post-growth processing that involves decorating Ge nanowires with Au and encapsulating them in graphitic carbon shells to support the melting and crystallization of alloy segments without disrupting the morphology of the nanowires. To demonstrate the generality of this approach, we extend it to the formation of axial Ge-AgGe and Ge-AuAgGe nanowire heterostructures. We show that the nanowire diameter – *via* modifications of the binary phase diagrams at the nanoscale[41,42] and composition-dependent changes to the structure of the alloy melts – can be used to control the type of metastable phases incorporated in the metallic alloy segments. Finally, we establish the formation of a

previously unknown metastable γ-AgGe phase in thin, axially segmented Ge-AgGe nanowire heterostructures.

2. Results and Discussion

2.1. Formation and metastable phase selection in Ge-AuGe, Ge-AgGe, and Ge-AuAgGe axial nanowire heterostructures

The process of forming axial heterostructures from Ge nanowires is summarized in Figure 1 (a). Monocrystalline Ge nanowires are coated at room temperature with ultrathin carbon and gold films, and are subsequently annealed to activate their transformation into axially segmented Ge-AuGe wires. Figures 1 (b)-(f) show *in-situ* TEM images of the evolution of a representative Ge nanowire with pre-deposited C and Au upon heating to 750°C. The bright-field TEM image of Figure 1 (b) illustrates the structure and morphology of the nanowire at room temperature prior to *in-situ* annealing. The Au-rich alloy nanoparticle at the nanowire tip (the VLS catalyst) is clearly distinguishable by its darker contrast. Higher magnification TEM images show the thin polycrystalline Au/C layers covering the nanowire surface (Figure 1 (b')). As the temperature is raised to 200°C (Figure 1(c), (c')) the Au film starts to dewet,[43] and it rearranges on the nanowire surface into larger interconnected Au-rich areas while leaving small Au clusters covering the entire nanowire. At temperatures above 300°C, ordered graphitic shells assemble on the surface by a mechanism described in detail in Refs. [44,45]. Briefly, in the presence of C, the Au in the VLS seed at the nanowire tip and small Au clusters on the nanowire surface catalyze the complete encapsulation of the nanowire and of its Au-rich tip in a multilayer shell of graphitic carbon. In parallel, at temperatures between 300°C and the eutectic point (~360°C for bulk AuGe) the accumulated Au in parts of the nanowire surface locally initiates surface melting as it alloys with Ge so that eutectic AuGe composition is reached. The liquid near-surface alloy regions collect progressively more Au from the nanowire surface until entire segments of the Ge wire reach eutectic composition and melt. As a result of this spontaneous alloying, the nanowire transforms into a heterostructure of

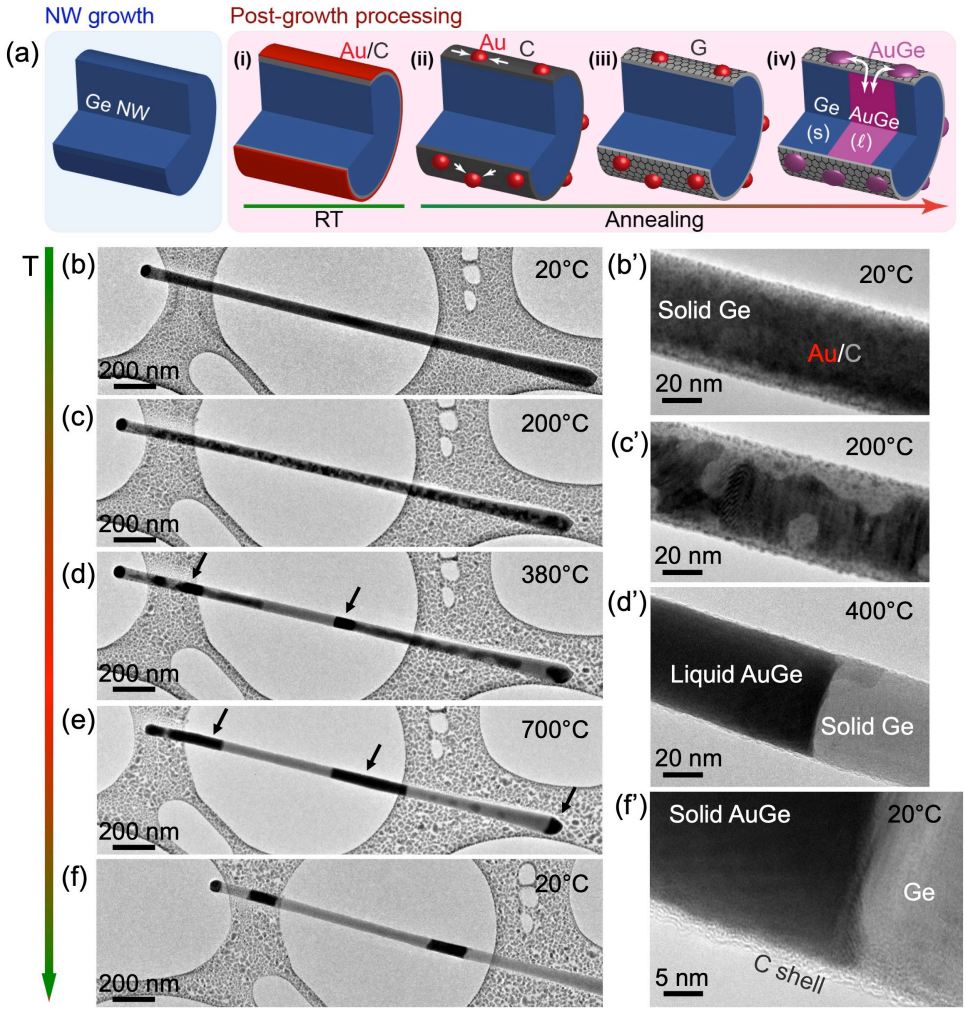

Figure 1. Formation of axially segmented (Ge, AuGe) nanowires via a liquid Au-Ge intermediate contained in a graphitic carbon shell, followed by crystallization in metastable γ- and β-AuGe phases. (a) Schematic showing the consecutive steps of transforming a single-crystalline Ge nanowire into an axial heterostructure by annealing in the presence of Au and C: (i) room temperature (RT) deposition of thin amorphous C and polycrystalline Au films; (ii) dewetting of the Au film into larger patches and nanoparticles; (iii) graphitization of the C film; (iv) alloying of Au and Ge to form expanding AuGe segments in the graphitic-C encapsulated Ge nanowires. **(b)** Representative Ge nanowire covered with C (1 nm) and Au (6 nm) at room temperature prior to the annealing experiments. **(b')** Higher magnification TEM image showing the nanowire at room temperature. **(c) – (e)** Sequence of TEM images of the nanowire obtained during annealing at temperatures between 20°C and 700°C. **(c')** Interface between a molten AuGe segment and the adjacent solid Ge. **(f)** Subsequent cooling of the segmented nanowire to room temperature and crystallization of the liquid AuGe segments. **(f')** High resolution TEM image of the crystalline Ge-AuGe interface at room temperature. Note the thin graphitic C-shell encapsulating the nanowire.

alternating segments of liquid AuGe (showing darker contrast) and solid Ge (lighter contrast, Figure 1 (d), (d')). The graphitic shell serves as a container for the AuGe liquid (Figure 1 (d') and (f')) and maintains a uniform nanowire shape and diameter despite the melting of the alloy segments. Holmberg et al. used carbon shells to contain AuGe melts in Ge nanowires,

for visualization by TEM at high temperatures.[46] Note that Au deposited on the carbon-terminated nanowire surface needs to cross the C-shell to be able to alloy with the Ge nanowire. Part of the Au uptake likely occurs early on, before an ordered graphitic shell has been formed, while even at later stages Au should be able to diffuse across the shell via defects, cracks, or domain boundaries. A further temperature increase causes the liquid AuGe segments to expand in length by incorporating additional Ge as the alloy traces its liquidus line and its equilibrium Ge content increases (Figure 1 (d), (e)). We previously showed a similar exchange of material across the solid Ge/liquid AuGe catalyst interface at the nanowire tip,[40,42,47] and established that the AuGe alloy closely follows the liquidus upon heating but remains Ge-rich (*i.e.*, deviates from the equilibrium composition) during the subsequent cooling. The liquid AuGe alloy segments formed here behave analogously. In particular, as the temperature is lowered they maintain higher than equilibrium Ge content and ultimately crystallize into segments of Ge-rich solid AuGe (Figure 1 (f), (f') – dark segments, see below) alternating with pure Ge segments (Figure 1 (f), (f') – light segments), thus forming an all-solid axial nanowire heterostructure. We found that the formation of axial heterostructures of alternating alloy (AuGe; AgGe, see below) and Ge segments was not limited to regions exposed to high-energy electrons during *in-situ* microscopy at high temperatures but also occurred in unexposed sample areas. Hence, electron-beam irradiation effects, such as the tightening of graphitic carbon shells around melt drops observed previously,[45] do not play a significant role here and the process outlined above will also give rise to axial heterostructures during *ex-situ* processing, in absence of an electron beam.

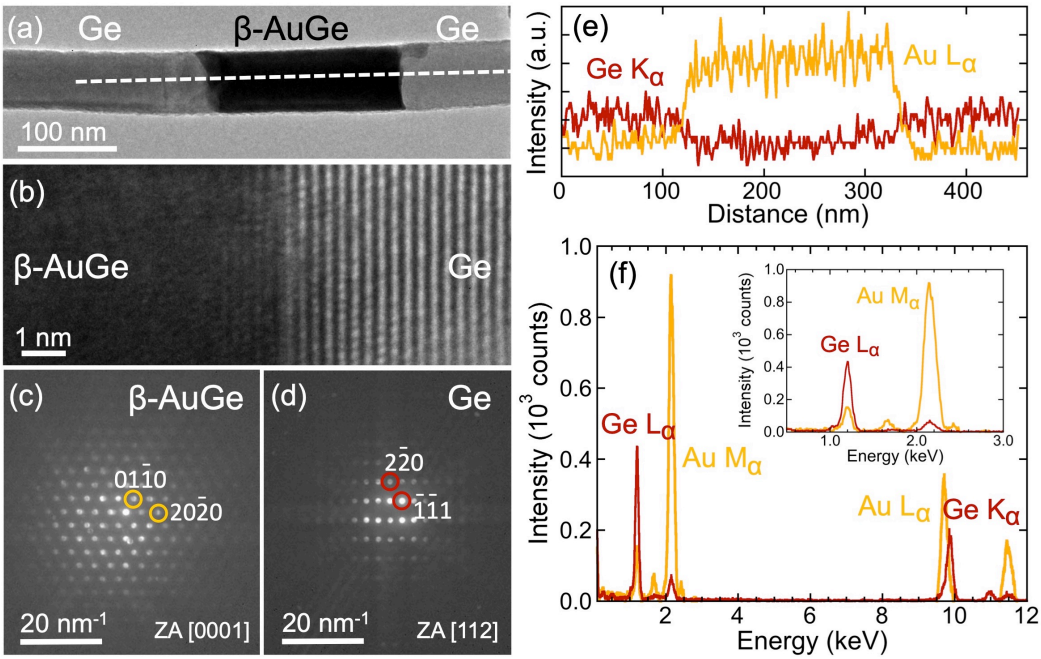

Figure 2. Thicker axially segmented Ge-AuGe nanowires (diameter d > 20 nm). (a) Typical TEM image of an axially segmented Ge-AuGe nanowire (~70 nm diameter). **(b)** High-resolution TEM image of the Ge-AuGe interface. **(c)** Nanobeam electron diffraction pattern of the areas with darker contrast in (a), indexed to the metastable β-AuGe phase. **(d)** Nanobeam electron diffraction pattern of the areas with lighter contrast in (a), indexed to crystalline Ge. Zone axes (ZA) are indicated in (c) and (d). **(e)** EDS line profiles of the relative intensity of Ge (red) and Au (yellow) along the line shown in (a). **(f)** EDS spectra obtained in the Ge (red) and AuGe (yellow) segments, respectively. Inset: Magnified view of the low-energy (Ge Lα, Au Mα) part of the spectra.

The segmented nanowires were further analyzed with focus on establishing the crystal structure of the AuGe alloy segments. Initial single crystalline VLS Ge nanowires with (111) lattice planes perpendicular to the wire axis and with diameters between 10-150 nm (Figure S1 – S3), were processed using the following protocol: Sequential coating with C and polycrystalline Au films (Figure 1 (b), (b')) with nominal thicknesses of 1 nm and 6 nm, respectively; and annealing at temperatures up to 750°C. For these conditions, we establish two distinct types of axial nanowire heterostructures, which comprise segments of two different metastable AuGe phases depending on the nanowire diameter, namely β-AuGe for wires above 20 nm diameter, and γ-AuGe for thinner wires (see below).

Figure 2 (a) shows a bright-field TEM image of part of a nanowire heterostructure (diameter d ~ 70 nm) containing a AuGe alloy segment (dark) sandwiched between Ge sections (bright).

High-angle annular dark field scanning TEM (HAADF-STEM, or Z-contrast) confirms a higher average atomic number (Z) in the segments with darker TEM contrast (Figure S4). High-resolution TEM (HRTEM, Figure 2 (b)) and nanobeam electron diffraction (Figure 2 (c), (d)) demonstrate that both types of segments are single crystals. The brighter areas consist of crystalline Ge (Figure 2 (d)); nanobeam diffraction patterns of the darker segments can be indexed to the metastable hexagonal β-AuGe phase (Zone axis: [0001]; Reported lattice parameters: a = 0.2853 nm, c = 0.4687 nm, Figure 2 (c)).[25] Energy dispersive X-ray spectroscopy (EDS) shows that the segments with lighter contrast contain mostly Ge, while an increased Au signal is detected in the β-AuGe segment (Figure 2 (e), (f)). The interfaces between Ge and AuGe segments are quite sharp. HRTEM shows an extent of the interface of the order of 4-5 Ge(111) lattice spacings, *i.e.*, 1.2 – 1.5 nm (Figure 2 (b)). Thicker Ge nanowires with diameters d > 20 nm processed as shown in Figure 1 invariably transform into axial nanowire heterostructures consisting of alternating Ge and metastable β-AuGe segments. Figure 3 (a) shows a representative thinner Ge-AuGe nanowire (diameter d ~ 19 nm). The lighter contrast in TEM again stems from crystalline Ge segments, while the darker segments can be assigned to the metastable γ-AuGe phase. The HRTEM image (Figure 3 (b)) and corresponding fast-Fourier transform (FFT, Figure 3 (c)) of the AuGe alloy show lattice spacings of 0.50(7) nm and 0.26(0) nm along two orthogonal directions, corresponding to the (211) and (420) lattice spacings of the bct γ-AuGe phase with space group $I4_1cd$, reported lattice constants a = 1.1627 nm, c = 2.2491 nm (Ref [48]) and Au and Ge atomic positions equivalent to the Cd and As positions in Cd_3As_2 crystal structure,[49] as suggested by ICDD file 00-018-0551.

From these combined findings, we conclude that the thermal process for creating axial nanowire heterostructures shown in Figure 1 invariably produces metastable AuGe segments, whose crystal phase is determined by the nanowire diameter. Under identical conditions, such

as nominal Au and C film thicknesses and annealing temperatures, thicker Ge nanowires (d > 20 nm) incorporate β-AuGe segments, while thin wires favor the formation of γ-AuGe segments.

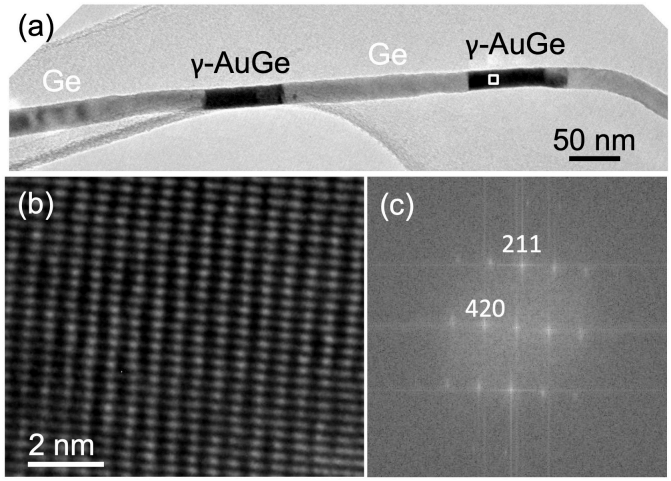

Figure 3. Thin axially segmented Ge-AuGe nanowires (diameter d < 20 nm). (a) Typical TEM image of an axially segmented Ge-AuGe nanowire (~19 nm diameter). **(b)** High-resolution TEM image of the AuGe alloy segment. **(c)** Fourier transform of the image in (b) indexed to the metastable γ -AuGe phase.

Similar to Au-Ge, Ag-Ge has a phase diagram of the eutectic type and forms metastable phases when rapidly quenched from the melt or subjected to high pressure.[25,35] For alloy compositions of Ag-(26 at.%) Ge, a hcp phase forms similar to the β-Au-(20 at.%) Ge phase. The Ag-(26 at.%) Ge hcp phase has a larger stability region with wider range both in temperature and composition. This phase is metastable in the bulk, but persists at room temperature after quenching of the melt. While AuGe alloys with higher Ge content (40-50 at.%) have been reported to crystallize in a second metastable phase, γ-AuGe,[32] no such phase has been observed for AgGe alloys. We used the process shown in Figure 1 for Au-Ge to investigate the formation of axial nanowire heterostructures containing segments of metastable Ag-Ge phases. Before annealing, Ag with nominal thickness of 5 nm or 10 nm was deposited on Ge nanowires with different diameters. The thin Ag films show a morphology and behavior during annealing similar to the Au films discussed above, *i.e.*, are initially polycrystalline and quasi-continuous (Figure S5 (a), (b)) but upon annealing above 200ºC

undergo dewetting. The Ag/C capped nanowires were slowly heated to 700°C *in-situ* in the TEM, above the eutectic temperature for bulk Ag-Ge (651°C) and significantly higher than the eutectic temperatures established for nanoscale Ag-Ge structures,[50] followed by natural cooling to room temperature. The observed behavior is analogous to that shown in Figure 1. Ge nanowires reacted with Ag at high temperatures invariably develop segments of metastable AgGe phases, *i.e.*, transform into axially segmented Ge-AgGe heterostructures. The characterization of the AgGe phases formed in Ge nanowires with different diameters is summarized below.

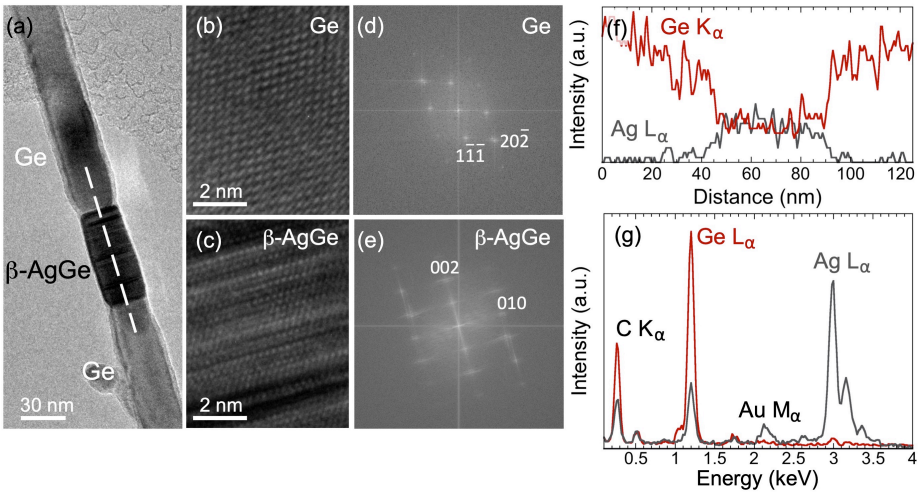

Figure 4. Thicker axially segmented Ge-AgGe nanowires (10 nm Ag). (a) Typical TEM image of an axially segmented Ge-AgGe nanowire (~40 nm diameter). **(b)-(c)** High resolution TEM images of the Ge and β-AgGe segments. **(d)** FFT analysis of the sections with lighter contrast in (a), indexed to crystalline Ge. **(e)** FFT analysis of the areas with darker contrast in (a), indexed to β-AgGe. **(f)** EDS line profiles of the relative intensities of Ge (red) and Ag (grey) along the line shown in (a). **(g)** Characteristic EDS spectra from the Ge (red line) and β-AgGe (grey line) segments in the axial nanowire heterostructure.

Whereas the AuGe segments discussed above approximately matched the volume of the replaced Ge nanowire section (*i.e.*, maintained a constant diameter), AgGe segments have higher density and hence a contracted diameter (Figure 4 (a); see also Figure 5 (a) and Figure 6 (a)). Such volume changes are easily accommodated by the thin graphitic C shell containing the melt at high temperatures. Combined HRTEM (Figure 4 (b)-(e)) and EDS analysis of this thicker Ge nanowire (d ~ 40 nm; Figure 4 (f), (g)) shows atomically sharp interfaces between the Ge and AgGe segments, alloy segments containing predominantly Ag and Ge and with

crystal structure identified as the metastable hexagonal β-AgGe phase. Metastable β-AgGe is found for all Ge nanowires with diameters d > 20 nm.

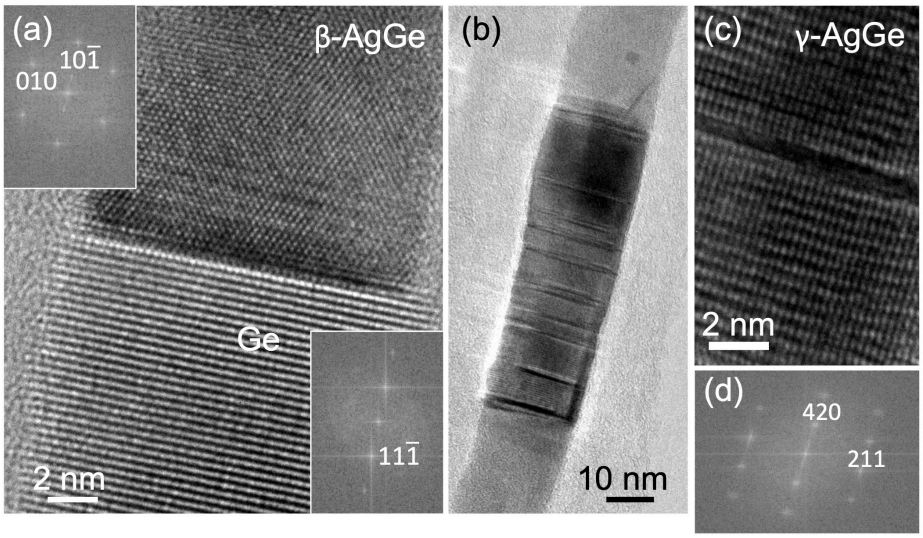

Figure 5. Thin axially segmented Ge-AgGe nanowires (diameter d < 20 nm). (a) High resolution TEM image of a nanowire with ~15 nm diameter and nominally 5 nm Ag. **(Inset – top left)** – FFT of the image of the segment to the right indexed to the β-AgGe metastable phase. **(Inset – bottom right)** – FFT of the Ge segment. **(b)** Typical TEM image of a nanowire with ~19 nm diameter, 10 nm Ag. **(c)** High-resolution TEM image of the AgGe alloy segment (dark contrast in (b)). **(d)** FFT of the high-resolution image in (c), indexed to the metastable γ-AgGe phase.

Processing thin Ge nanowires decorated with 5 nm Ag produces alloy segments that crystallize into β-AgGe, similar to thicker wires (Figure 5 (a)). However, larger amounts of deposited Ag (10 nm) lead to a different metastable structure. Figure 5 (b) shows a typical AgGe segment in a Ge nanowire with ~19 nm diameter. Its structure, observed by HRTEM (Figure 5 (c)), does not match β-AgGe. Comparison with high-resolution images of γ-AuGe (Figure 3 (b), (c)) shows close similarities. In particular, the new AgGe phase has lattice spacings of 0.507 nm and 0.260 nm, identical to the (211) and (420) lattice spacings of the bct γ-AuGe phase (Figure 3 (b), (c)).[49] These findings strongly suggest that metastable γ-AgGe can form in nanowires, even though such a structure has never been observed for bulk AgGe alloys.

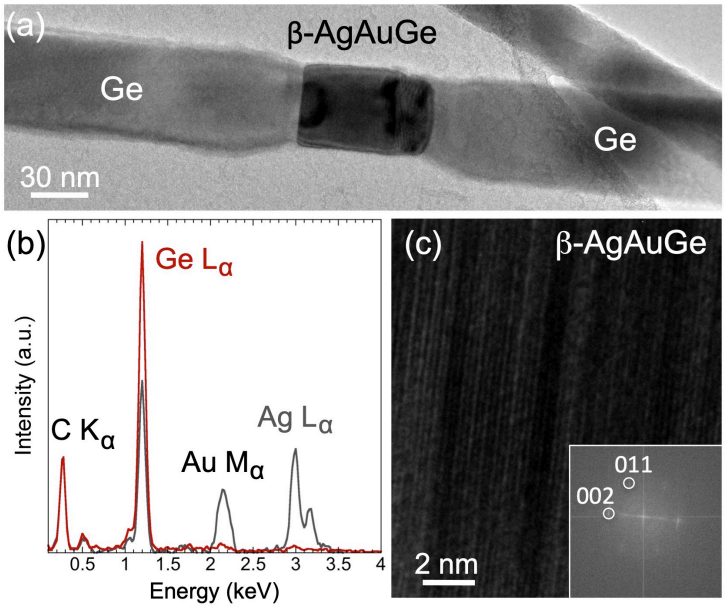

Figure 6. Axially segmented Ge-ternary (AuAgGe) nanowires. (a) TEM image of the axial nanowire heterostructure (d_{Ge} ~ 53 nm). **(b)** Characteristic EDS spectra from the Ge (red line) and β-AuAgGe (grey line) segments in the nanowire shown in (a). **(c)** HRTEM image of the β-AgAuGe segment. **(Inset – bottom right)** – FFT of the image in (b) indexed to the β-AgGe metastable phase.

The hexagonal β-AuGe (a = 0.2853 nm, c = 0.4687 nm, Ref. [25]) and β-AgGe (a = 0.2860 nm, c = 0.4666 nm, Ref. [25]) phases are isostructural with nearly identical lattice constants and are thus expected to be completely soluble across all compositions. This offers the possibility of forming ternary solid solutions in nanowire heterostructures. To realize such materials, Ge nanowires were decorated with both Au and Ag at room temperature and annealed to form axial alloy segments (Figure 6 (a)). EDS confirms that these segments indeed contain Ag and Au (Figure 6 (b)). HRTEM (Figure 6 (c)) shows that the ternary alloy segments are single-crystalline with a plane spacing of 0.24(7) nm, consistent with the (100) lattice plane spacing of β-AuGe and β-AgGe. The interfaces between the ternary AuAgGe alloy and Ge are atomically sharp, and EDS shows no detectable Au or Ag in the Ge segments of the heterostructures.

2.2. Selection mechanism of different metastable phases: Structure of the melt

The selection of different metastable AuGe phases in axially segmented nanowires is consistent with our prior work, where we demonstrated that the solubility of Ge in AuGe melt

drops at the tips of VLS nanowires is dependent on the nanowire diameter, with AuGe drops on thinner wires showing higher Ge solubility due to a size-dependent depression of the AuGe liquidus.[41,42] A higher solubility of Ge correlated with a preference for crystallization into metastable γ-AuGe upon cooling.[40] Alloy segments in axial nanowire heterostructures show analogous behavior, *i.e.*, thicker wires form segments of β-AuGe, while thin wires with higher Ge solubility in the AuGe melt produce γ-AuGe segments. Thus, for identical process conditions (amount of added Au, annealing temperature) the nanowire diameter controls the type of metastable phase in the AuGe alloy segments of the axial AuGe-Ge nanowire heterostructures. We carried out additional experiments to probe possible differences in the structural motifs of AuGe melts close to the eutectic composition (crystallizing as β-AuGe) and in the Ge-rich regime (crystallizing as γ-AuGe), which could explain the phase selection during crystallization. A correlation between the structure of the melt and the solid crystal phase was found in previous work on the crystallization of Ga nanodrops.[51] Experimental data on the structure and crystallization of nanometer-sized metallic melt drops remain scarce,[45] and these systems tend to be too large for atomistic simulations over relevant time scales.

We performed electron diffraction on AuGe melt drops at the tips of Ge nanowires to determine the liquid structure factor in Ge-rich AuGe melts, for which there are no experimental data available in the literature.[52] Diffraction measurements on the nanowire tips are representative of the behavior of AuGe melts in embedded axial segments along the nanowires, as shown by a direct comparison of segment- and tip-melts in Figure S6. Ge-rich melts are achieved by heating Ge nanowires with AuGe VLS seeds to temperatures well

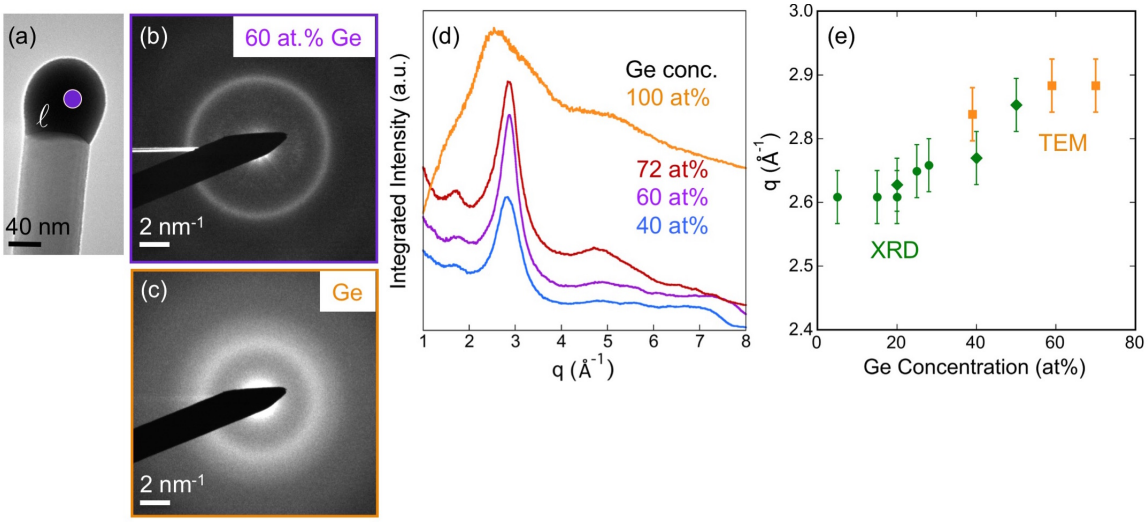

Figure 7: Electron diffraction of liquid AuGe drops at the tips of Ge nanowires. (a) TEM image of the Ge nanowire and AuGe melt drop at its tip at temperatures above 360°C. **(b)** Diffraction pattern from the AuGe drop at 515°C, exhibiting diffuse rings. **(c)** Diffraction pattern from a supercooled Ge drop, obtained at 880°C showing a broader primary ring at smaller spatial frequency than in AuGe. **(d)** Radial distribution of the diffracted intensity of liquid Ge, compared with AuGe melts at different temperatures, i.e. with different Ge content. **(e)** Position of the principal diffraction peak as a function of composition (see (d)), compared to the results obtained by X-ray diffraction on bulk AuGe melts.[53,54]

above the eutectic point (Figure 7 (a)),[41,42] where the alloy adjusts its composition by incorporating Ge from the adjacent solid Ge reservoir (*i.e.*, traces the liquidus line). The composition can be inferred from *in-situ* TEM observations of the drop and of the advancing interface to the Ge wire.[41,42] Figure 7 (a) shows a TEM image of a AuGe melt drop at the tip of a Ge nanowire at T = 515°C. The corresponding selected-area electron diffraction pattern obtained within the melt drop (Figure 7 (b)) consists of diffuse rings, characteristic of the liquid phase. Figure 7 (d) shows the radial distributions of the diffracted intensity of the AuGe melt at three different temperatures (*i.e.*, different Ge content).[41,42] Electron diffraction on AuGe drops was compared to measurements on large Ge particles, which were briefly brought to the melting temperature and then supercooled to ~880°C where electron diffraction patterns were obtained (Figure 7 (c)). The radial distribution of diffracted intensity of the pure Ge melt is shown in Figure 7 (d). Comparison to the structure factor determined by X-ray diffraction of bulk liquid Ge[52] shows a good correlation in both the overall curves as well as the positions of the principal peaks, validating the use of electron diffraction for investigating

the structure of melts. In contrast to pure Ge, which shows a broad diffuse diffraction ring at q ~2.5 $Å^{-1}$, Ge-rich AuGe melts are characterized by a narrower primary peak with a shoulder towards larger q-vectors, consistent with X-ray structure factors of liquid bulk AuGe with lower Ge content.[53-55] Increasing the Ge content shifts this principal peak systematically toward larger q (Figure 7 (e), orange squares), continuing a trend observed in X-ray diffraction at lower Ge concentration (Figure 7 (e), green circles[53] and diamonds[54,55]). The same is also observed in the direct comparison of diffraction patterns and radial intensity distributions of AuGe segments embedded in thick and thin wires where the principal diffraction peak of AuGe melts in thinner nanowires, which are expected to reach higher Ge concentration at the same temperature, systematically shifts to larger q (Figure S7). X-ray diffraction on bulk AuGe melts shows a simple close-packed liquid structure, similar to that of Au, for AuGe melts near the eutectic point (*i.e.*, 28 at.% Ge).[56] With increasing Ge concentration (50 at.% Ge), a clear trend to a more open structure – characteristic of liquid group IVA elements – emerges.[56,57] Splat-cooling of such Ge-rich bulk AuGe melts, which tends to produce crystalline structures templated by the packing in the liquid, results in metastable γ-AuGe, *i.e.*, the same phase crystallized in our experiments from slowly supercooled AuGe melts with high Ge content inserted into Ge nanowires. The notion that the underlying liquid-phase structural motifs of the Ge-rich AuGe melt are preserved during supercooling in a nanoscale system, whereas they can only be quenched-in at very high cooling rates in the bulk, indicates a that these liquid phase motifs can be stabilized during supercooling of nanoscale melts.

3. Conclusions

In-situ TEM investigations show that Ge nanowires decorated with Au (Ag) spontaneously transform into axial nanowire heterostructures consisting of metastable metallic AuGe (AgGe) segments alternating with semiconducting Ge segments. In the axial heterostructures formed here, the length and spacing of the inserted metallic AuGe and AgGe alloy segments

did not show any pronounced ordering, *i.e.*, they were likely dictated by local differences in the supply and mass transport of Ge and metal, permeability of the graphitic carbon shell, *etc*. If such non-uniformities can be eliminated, the combination of our thermal process with self-organization phenomena, such as a Plateau-Rayleigh instability, could provide a pathway toward highly ordered axial segmentation of nanowires. The type of the metastable phase in the metallic segments, hexagonal β-AuGe (β-AgGe) or tetragonal γ-AuGe (γ-AgGe), which forms during slow cooling of molten binary AuGe (AgGe) alloys contained in graphitic carbon shells is governed by the Ge nanowire diameter. Size effects generally cause an enhanced solubility of Ge in nanoscale melts compared to the bulk. Electron diffraction on AuGe melt drops at the nanowire tips suggests that structural motifs in the liquid play a role in templating the crystalline metastable phase that is obtained. These findings provide the foundation for harnessing the functional properties of metastable phases in nanowires and other nanoscale systems.

4. Methods

Ge nanowires with a broad distribution of diameters were synthesized by vapor-liquid-solid (VLS) growth *via* digermane (Ge_2H_6) chemical vapor deposition over Au catalysts formed by thermally dewetting thin Au films (2 nm nominal thickness) on Ge (100) substrates. VLS growth was performed at ~380°C in an ultrahigh vacuum reactor with a base pressure of 2×10^{-9} Torr.[43,47] The diameters of the resulting single-crystalline Ge nanowires ranged from 10 nm to ~150 nm. As-grown Ge nanowires were dispersed on amorphous carbon films supported by standard Cu, Au or W TEM grids for the variable-temperature *in-situ* TEM experiments. Immediately before transfer to the TEM, a 1 nm C film followed by nominally 2-10 nm Au or Ag films were deposited on the dispersed Ge nanowires by sputtering at room temperature, which results in polycrystalline Au or Ag films on the nanowire surface (See Figures 1 and S4). The morphology and composition of individual nanowires was investigated by TEM, HAADF-STEM, as well as selected-area and nanobeam electron diffraction in JEOL

2100F and FEI Talos F200X field emission microscopes, equipped with an energy dispersive x-ray (EDS) detector, at an electron-beam energy of 200 keV. Variable-temperature *in-situ* TEM experiments used a Gatan 652 single tilt high-temperature holder and covered the temperature range between room temperature and 800°C while maintaining pressures below 10^{-7} Torr. The electron intensity was kept intentionally low (< 0.1 A/cm^2) to prevent any uncontrolled electron beam-induced structural changes. The AuGe alloy composition for the investigation of liquid structural motifs as a function of temperature and Ge content was quantified from measurements of the volume of VLS seed drops at the tips of Ge nanowires, following a procedure described in detail previously.[40,42,47]

Supporting Information Available. Supporting Figures S1-S7: TEM imaging and diffraction analysis of the initial Ge nanowires; crystal structure of thin Ge nanowires; TEM and STEM of an axially segmented Ge-AuGe nanowire heterostructure; TEM characterization of Ge nanowires with deposited C and Ag films, before and after annealing; comparison of electron diffraction patterns of AuGe melts at nanowire tips and in axial segments, and of AuGe segments in thick and thin Ge nanowires.

Conflicts of Interest. The authors declare that they have no conflicts of interest.

Acknowledgements

This work was supported by the National Science Foundation, Division of Materials Research, Solid State and Materials Chemistry Program under Grant No. DMR-1607795.

References

1. Elmalem, E.; Saunders, A. E.; Costi, R.; Salant, A.; Banin, U. Growth of Photocatalytic CdSe-Pt Nanorods and Nanonets. *Adv Mater* **2008,** 20, 4312-4317.
2. Li, P.; Wei, Z.; Wu, T.; Peng, Q.; Li, Y. Au−ZnO Hybrid Nanopyramids and Their Photocatalytic Properties. *Journal of the American Chemical Society* **2011,** 133, 5660-5663.
3. Hong, X.; Yin, Z.; Fan, Z.; Tay, Y. Y.; Chen, J.; Du, Y.; Xue, C.; Chen, H.; Zhang, H. Periodic AuAg‐Ag2S Heterostructured Nanowires. *Small* **2014,** 10, 479-482.
4. Jiang, R.; Li, B.; Fang, C.; Wang, J. Metal/Semiconductor Hybrid Nanostructures for Plasmon‐Enhanced Applications. *Adv Mater* **2014,** 26, 5274-5309.
5. Orrù, M.; Rubini, S.; Roddaro, S. Formation of axial metal–semiconductor junctions in GaAs nanowires by thermal annealing. *Semiconductor Science and Technology* **2014,** 29, 054001.
6. Wang, X.; Ozkan, C. S. Multisegment Nanowire Sensors for the Detection of DNA Molecules. *Nano Letters* **2008,** 8, 398-404.
7. Zhang, A.; Lieber, C. M. Nano-Bioelectronics. *Chemical Reviews* **2016,** 116, 215-257.
8. Gur, I.; Fromer, N. A.; Geier, M. L.; Alivisatos, A. P. Air-Stable All-Inorganic Nanocrystal Solar Cells Processed from Solution. *Science* **2005,** 310, 462-465.
9. Hwang, Y. J.; Boukai, A.; Yang, P. High Density n-Si/n-TiO2 Core/Shell Nanowire Arrays with Enhanced Photoactivity. *Nano Letters* **2009,** 9, 410-415.
10. Sutter, E.; Camino, F.; Sutter, P. One-step synthesis of Ge-SiO2 core-shell nanowires. *Appl Phys Lett* **2009,** 94, 083109.
11. Koenigsmann, C.; Sutter, E.; Chiesa, T. A.; Adzic, R. R.; Wong, S. S. Highly Enhanced Electrocatalytic Oxygen Reduction Performance Observed in Bimetallic Palladium-Based Nanowires Prepared under Ambient, Surfactantless Conditions. *Nano Letters* **2012,** 12, 2013-2020.
12. Peng, X.; Santulli, A. C.; Sutter, E.; Wong, S. S. Fabrication and enhanced photocatalytic activity of inorganic core-shell nanofibers produced by coaxial electrospinning. *Chemical Science* **2012,** 3, 1262-1272.
13. Koenigsmann, C.; Tan, Z.; Peng, H.; Sutter, E.; Jacobskind, J.; Wong, S. S. Multifunctional Nanochemistry: Ambient, Electroless, Template‐Based Synthesis and Characterization of Segmented Bimetallic Pd/Au and Pd/Pt Nanowires as High‐Performance Electrocatalysts and Nanomotors. *Israel Journal of Chemistry* **2012,** 52, 1090-1103.
14. Berganza, E.; Jaafar, M.; Bran, C.; Fernández-Roldán, J. A.; Chubykalo-Fesenko, O.; Vázquez, M.; Asenjo, A. Multisegmented Nanowires: a Step towards the Control of the Domain Wall Configuration. *Scientific Reports* **2017,** 7, 11576.
15. Hong, X.; Yin, Z.; Fan, Z.; Tay, Y.-Y.; Chen, J.; Du, Y.; Xue, C.; Chen, H.; Zhang, H. Periodic AuAg-Ag2S Heterostructured Nanowires. *Small* **2014,** 10, 479-482.
16. Gudiksen, M. S.; Lauhon, L. J.; Wang, J.; Smith, D. C.; Lieber, C. M. Growth of nanowire superlattice structures for nanoscale photonics and electronics. *Nature* **2002,** 415, 617.
17. Mouchet, C.; Latu-Romain, L.; Cayron, C.; Rouviere, E.; Celle, C.; Simonato, J.-P. Growth of one-dimensional Si/SiGe heterostructures by thermal CVD. *Nanotechnology* **2008,** 19, 335603.
18. Carnevale, S. D.; Yang, J.; Phillips, P. J.; Mills, M. J.; Myers, R. C. Three-Dimensional GaN/AlN Nanowire Heterostructures by Separating Nucleation and Growth Processes. *Nano Letters* **2011,** 11, 866-871.

19. Johansson, J.; Dick, K. A. Recent advances in semiconductor nanowire heterostructures. *Crystengcomm* **2011,** 13, 7175-7184.
20. Li, D.; Wu, Y.; Fan, R.; Yang, P.; Majumdar, A. Thermal conductivity of Si/SiGe superlattice nanowires. *Appl Phys Lett* **2003,** 83, 3186-3188.
21. Wallentin, J.; Ek, M.; Vainorious, N.; Mergenthaler, K.; Samuelson, L.; Pistol, M.-E.; Reine Wallenberg, L.; Borgström, M. T. Semiconductor-Oxide Heterostructured Nanowires Using Postgrowth Oxidation. *Nano Letters* **2013,** 13, 5961-5966.
22. Li, X.; Meng, G.; Qin, S.; Xu, Q.; Chu, Z.; Zhu, X.; Kong, M.; Li, A.-P. Nanochannel-Directed Growth of Multi-Segment Nanowire Heterojunctions of Metallic Au1–xGex and Semiconducting Ge. *ACS Nano* **2012,** 6, 831-836.
23. Steiner, D.; Mokari, T.; Banin, U.; Millo, O. Electronic Structure of Metal-Semiconductor Nanojunctions in Gold CdSe Nanodumbbells. *Phys Rev Lett* **2005,** 95, 056805.
24. Mongin, D.; Shaviv, E.; Maioli, P.; Crut, A.; Banin, U.; Del Fatti, N.; Vallée, F. Ultrafast Photoinduced Charge Separation in Metal–Semiconductor Nanohybrids. *ACS Nano* **2012,** 6, 7034-7043.
25. Fujinaga, Y.; Kusaba, K.; Syono, Y.; Iwasaki, H.; Kikegawa, T. Formation of an Intermediate Phase in Eutectic Au-Ge and Ag-Ge Systems under High-Pressure. *J Less-Common Met* **1991,** 170, 277-286.
26. Predel, B., *Phase Equilibria. In Crystallographic and Thermodynamic Data of Binary Alloys – Electronic Materials and Semiconductors, Landolt-Bornstein, Group IV: Physical Chemistry*. Springer: Berlin, 1998; Vol. 5.
27. Okamoto, H.; Massalski, T. B. The Au−Ge (Gold-Germanium) system. *Bulletin of Alloy Phase Diagrams* **1984,** 5, 601-610.
28. Woodruff, J. H.; Ratchford, J. B.; Goldthorpe, I. A.; McIntyre, P. C.; Chidsey. Vertically Oriented Germanium Nanowires Grown from Gold Colloids on Silicon Substrates and Subsequent Gold Removal. *Nano Letters* **2007,** 7, 1637-1642.
29. Dayeh, S. A.; Picraux, S. T. Direct Observation of Nanoscale Size Effects in Ge Semiconductor Nanowire Growth. *Nano Letters* **2010,** 10, 4032-4039.
30. Hanrath, T.; Korgel, B. A. Chemical Surface Passivation of Ge Nanowires. *Journal of the American Chemical Society* **2004,** 126, 15466-15472.
31. Biswas, S.; O'Regan, C.; Petkov, N.; Morris, M. A.; Holmes, J. D. Manipulating the Growth Kinetics of Vapor-Liquid-Solid Propagated Ge Nanowires. *Nano Letters* **2013,** 13, 4044-4052.
32. Anatharaman, T. R.; Luo, H. L.; Klement, W. Nonequilibrium Structures in Gold-Germanium Alloys. *T Metall Soc Aime* **1965,** 233, 2014.
33. Duwez, P.; Willens, R. H.; Klement, W. Metastable Electron Compound in Ag-Ge Alloys. *J Appl Phys* **1960,** 31, 1137-1137.
34. Ananthar.Tr; Luo, H. L.; Klement, W. Formation of New Intermetallic Phases in Binary Eutectic Systems by Drastic Undercooling of Melt. *Nature* **1966,** 210, 1040-1040.
35. Chipenko, G. V.; Degtyareva, V. F. Formation of Hume-Rothery phases in Ag-Ge and Au-Ge alloys by application of high pressures *Soviet Physics - Solid State* **1984,** 26, 735-6.
36. Klement, W. Lattice Parameters of the Metastable Close-Packed Structures in Silver Germanium Alloys. *J I Met* **1961,** 90, 27-30.
37. Gamalski, A. D.; Tersoff, J.; Sharma, R.; Ducati, C.; Hofmann, S. Metastable Crystalline AuGe Catalysts Formed During Isothermal Germanium Nanowire Growth. *Phys Rev Lett* **2012,** 108, 255702.
38. Rath, A.; Dash, J. K.; Juluri, R. R.; Ghosh, A.; Grieb, T.; Schowalter, M.; Krause, F. F.; Muller, K.; Rosenauer, A.; Satyam, P. V. A study of the initial stages of the growth of

Au-assisted epitaxial Ge nanowires on a clean Ge(100) surface. *Crystengcomm* **2014,** 16, 2486-2490.
39. Lu, H.; Meng, X. Nanophase diagram of binary eutectic Au-Ge nanoalloys for vapor-liquid-solid semiconductor nanowires growth. *Scientific Reports* **2015,** 5, 11263.
40. Sutter, E.; Sutter, P. Formation and stabilization of single-crystalline metastable AuGe phases in Ge nanowires. *Nanotechnology* **2011,** 22, 295605.
41. Sutter, E. A.; Sutter, P. W. Size-Dependent Phase Diagram of Nanoscale Alloy Drops Used in Vapor−Liquid−Solid Growth of Semiconductor Nanowires. *ACS Nano* **2010,** 4, 4943-4947.
42. Sutter, E.; Sutter, P. Phase Diagram of Nanoscale Alloy Particles Used for Vapor−Liquid−Solid Growth of Semiconductor Nanowires. *Nano Letters* **2008,** 8, 411-414.
43. Sutter, E.; Ozturk, B.; Sutter, P. Selective growth of Ge nanowires by low-temperature thermal evaporation. *Nanotechnology* **2008,** 19.
44. Sutter, E.; Sutter, P. Au-induced encapsulation of Ge nanowires in protective C shells. *Adv Mater* **2006,** 18, 2583-2588.
45. Sutter, P. W.; Sutter, E. A. Dispensing and surface-induced crystallization of zeptolitre liquid metal-alloy drops. *Nat Mater* **2007,** 6, 363-366.
46. Holmberg, V. C.; Panthani, M. G.; Korgel, B. A. Phase Transitions, Melting Dynamics, and Solid-State Diffusion in a Nano Test Tube. *Science* **2009,** 326, 405-407.
47. Sutter, E. A.; Sutter, P. W. Size-Dependent Phase Diagram of Nanoscale Alloy Drops Used in Vapor-Liquid-Solid Growth of Semiconductor Nanowires. *Acs Nano* **2010,** 4, 4943-4947.
48. International Center for Diffraction Data, ICDD 00-018-0551.
49. Ali, M. N.; Gibson, Q.; Jeon, S.; Zhou, B. B.; Yazdani, A.; Cava, R. J. The Crystal and Electronic Structures of Cd3As2, the Three-Dimensional Electronic Analogue of Graphene. *Inorganic Chemistry* **2014,** 53, 4062-4067.
50. Kryshtal, A.; Minenkov, A.; Bogatyrenko, S.; Gruszczyński, A. Melting process and the size depression of the eutectic temperature in Ag/Ge and Ge/Ag/Ge layered films. *Journal of Alloys and Compounds* **2019,** 786, 817-825.
51. Sutter, E. A.; Sutter, P. W.; Uccelli, E.; Morral, A. F. I. Supercooling of nanoscale Ga drops with controlled impurity levels. *Phys Rev B* **2011,** 84.
52. Kawakita, Y.; Takeda, S.; Enosaki, T.; Oshima, K.; Aoki, H.; Masaki, T.; Itami, T. Structure of liquid Ge at high temperatures. *J Phys Soc Jpn* **2002,** 71, 12-14.
53. Hoyer, W.; Jodicke, R. Short-Range and Medium-Range Order in Liquid Au-Ge Alloys. *J Non-Cryst Solids* **1995,** 193, 102-105.
54. Takeda, S.; Fujii, H.; Kawakita, Y.; Tahara, S.; Nakashima, S.; Kohara, S.; Itou, M. Structure of eutectic alloys of Au with Si and Ge. *Journal of Alloys and Compounds* **2008,** 452, 149-153.
55. Chirawatkul, P.; Zeidler, A.; Salmon, P. S.; Takeda, S.; Kawakita, Y.; Usuki, T.; Fischer, H. E. Structure of eutectic liquids in the Au-Si, Au-Ge, and Ag-Ge binary systems by neutron diffraction. *Phys Rev B* **2011,** 83, 014203.
56. Waghorne, R. M.; Rivlin, V. G.; Williams, G. I. Structure of liquid alloys of the Au-Si and Au-Ge systems. *Journal of Physics F: Metal Physics* **1976,** 6, 147-156.
57. Rivlin, V. G.; Waghorne, R. M.; Williams, G. I. The structure of gold alloys in the liquid state. *Gold Bulletin* **1976,** 9, 84 - 87.

Table of Contents Graphic

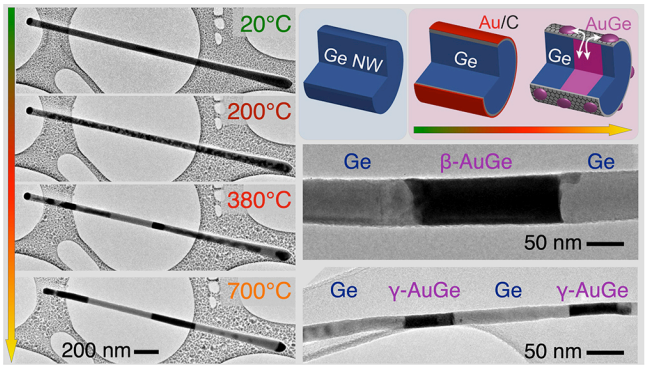

Supplementary Online Material

Axial heterostructures with phase-controlled metastable segments via post-growth reactions of Ge nanowires

Eli Sutter[1] and Peter Sutter[2]

[1]*Department of Mechanical and Materials Engineering, University of Nebraska-Lincoln, Lincoln, NE 68588 (USA)*
[2]*Department of Electrical and Computer Engineering, University of Nebraska-Lincoln, Lincoln, NE 68588 (USA)*

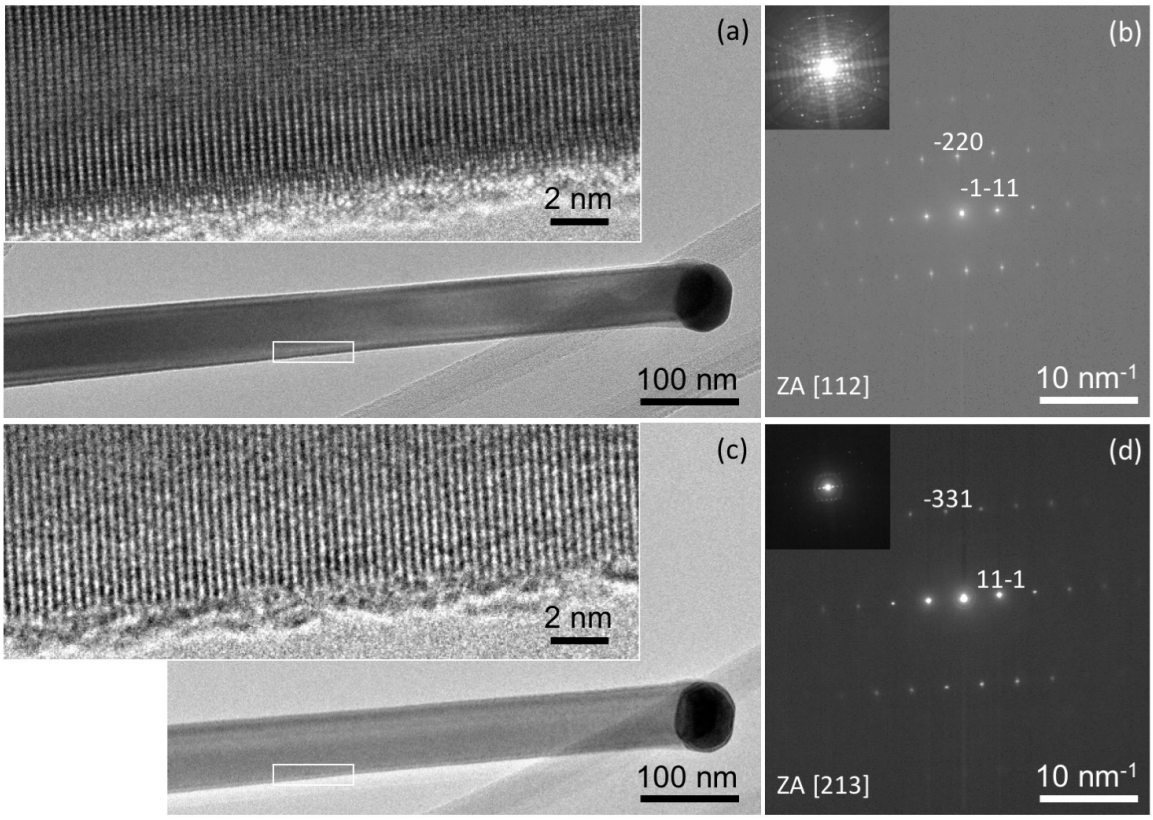

Figure S1. Morphology of a characteristic Ge nanowire. (a) TEM image of a typical Ge nanowire along the [112] zone axis. Inset: High-resolution TEM image of the nanowire part marked by the white rectangular frame in (a). **(b)** Selected area electron diffraction of the nanowire recorded along the [112] zone axis. Inset: Nanobeam electron diffraction pattern. **(c)** TEM image of the Ge nanowire after tilting by 11° to the [213] zone axis. Inset: High-resolution TEM image of the nanowire part marked by the white rectangular frame in (c). **(d)** Selected area electron diffraction of the nanowire recorded along the [213] zone axis. Inset: Nanobeam electron diffraction pattern. Zone axes (ZA) are indicated in (b) and (d).

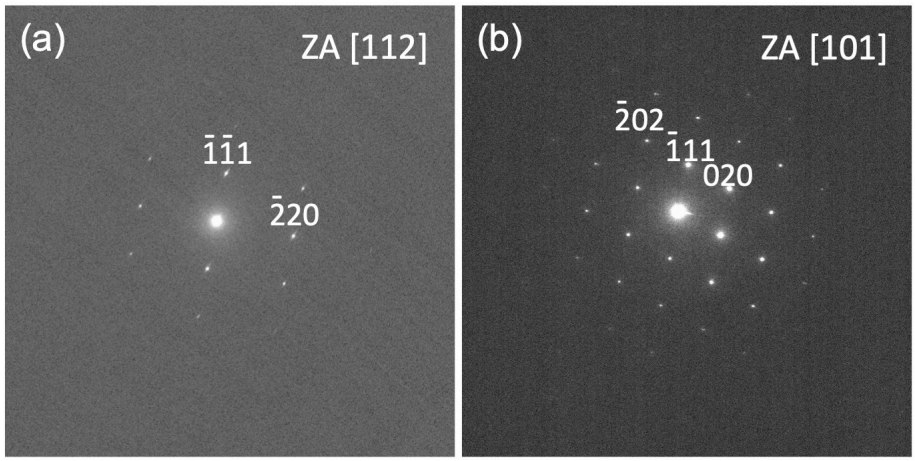

Figure S2. Electron diffraction on Ge nanowires along two different zone axes (ZA). (a) Diffraction pattern of a Ge nanowire along [112] zone axis. **(b)** Diffraction pattern of a Ge nanowire along [101] zone axis. Both patterns are indexed to single-crystalline Ge.

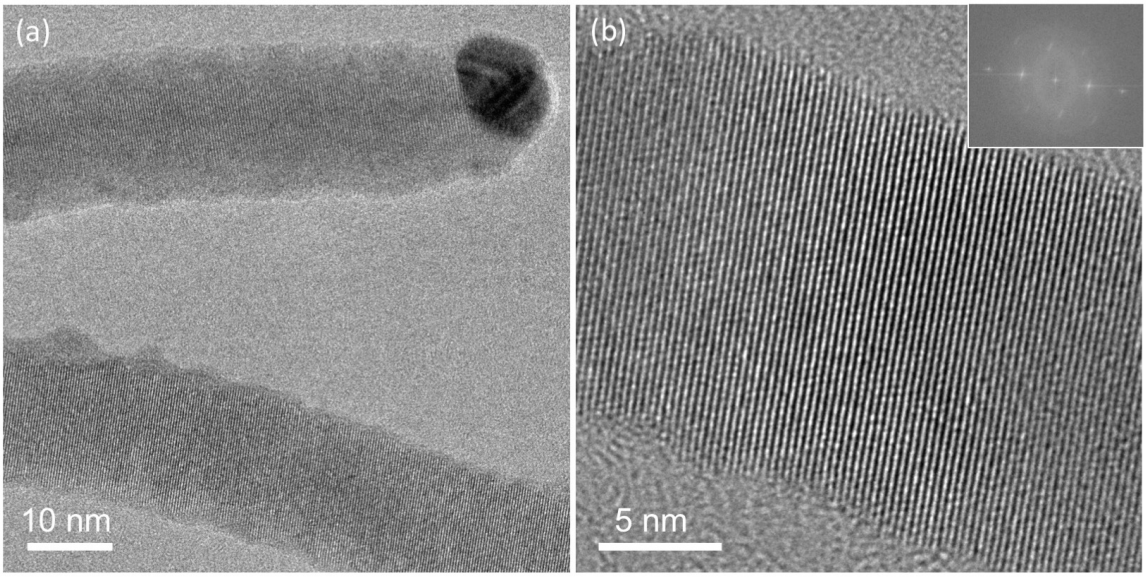

Figure S3. Crystal structure of Ge nanowires with diameters < 20 nm. (a) High-resolution TEM image of two Ge nanowires (~15 nm diameter). Both wires show {111} planes perpendicular to the nanowire axis. **(b)** Higher magnification TEM image of part of the lower nanowire in (a) showing the [111] growth direction of the nanowire. Inset (top right): FFT of (b).

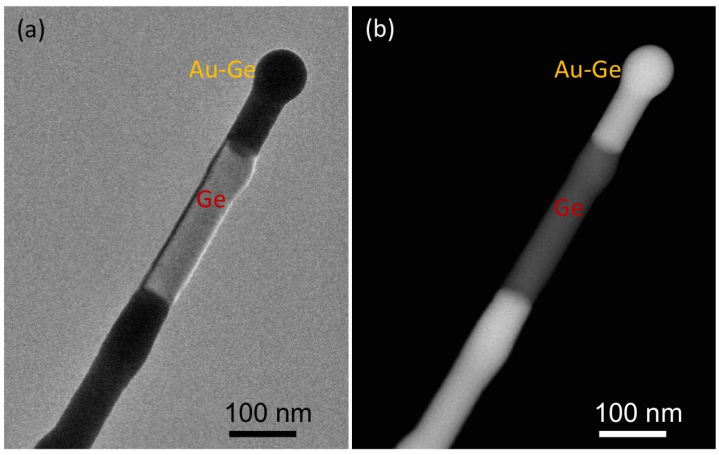

Figure S4. Ge-AuGe axial nanowire heterostructures. (a) TEM image of a segmented Ge-AuGe nanowire. **(b)** HAADF STEM (Z-contrast) image of the same nanowire.

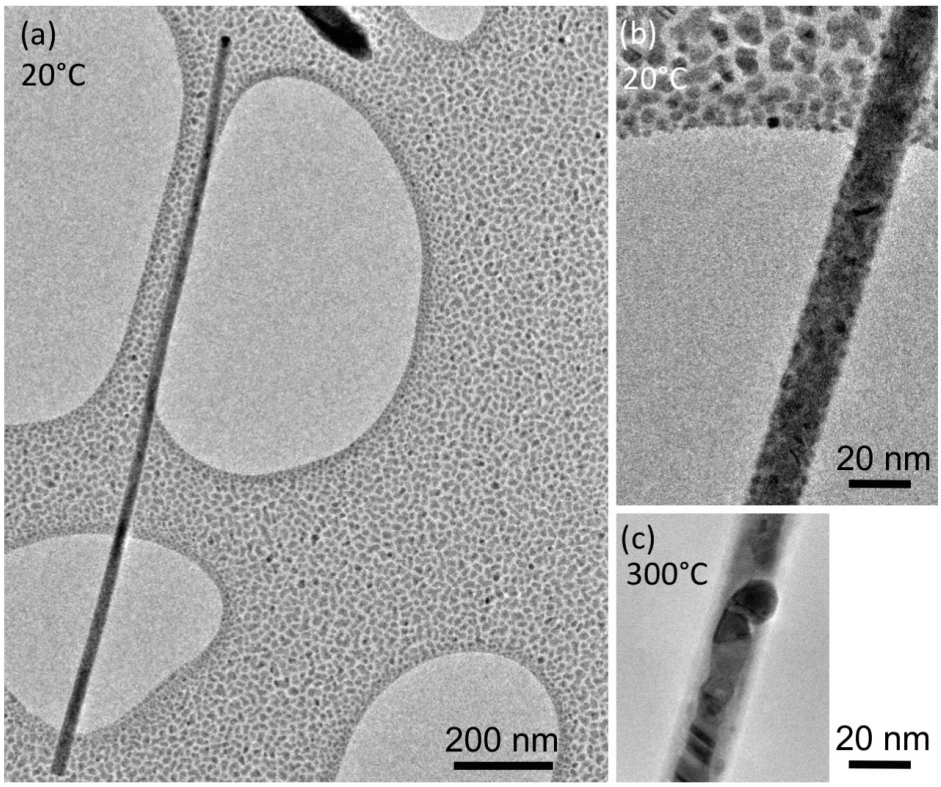

Figure S5. (a) Typical TEM image of a Ge nanowire on amorphous carbon grid after deposition of ~ 1 nm thick carbon film and 5 nm Ag at room temperature. The Ag film is polycrystalline and quasi-continuous. **(b)** Higher magnification TEM image of the nanowire showing the polycrystalline Ag film on its surface. **(c)** TEM image of a section of the same nanowire at 300°C showing the rearranging of the Ag on its surface.

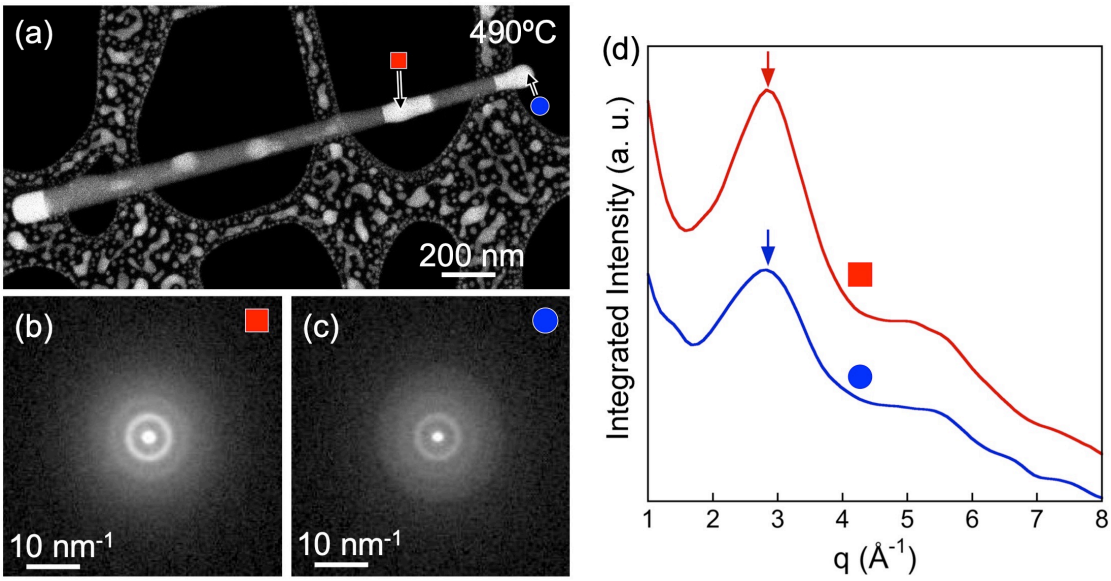

Figure S6. Comparison of nanobeam electron diffraction on AuGe melts at the nanowire tip and in alloy melt segments. (a) TEM image of an axially segmented nanowire (65 nm diameter) during annealing at 490°C. Liquid AuGe melt segments are imaged with bright contrast, whereas Ge segments appear dark. **(b)** High-temperature electron diffraction pattern (T = 490°C) from the AuGe melt segment, obtained at the position marked by a red square in (a). **(c)** High-temperature electron diffraction pattern (T = 490°C) from the AuGe melt drop at the nanowire tip, obtained at the position marked by a blue circle in (a). **(d)** Radial distribution of the diffracted intensity of the liquid AuGe melts at the two positions along the nanowire (tip: blue circle; internal segment: red square) showing identical positions of the principal diffraction peak (arrows).

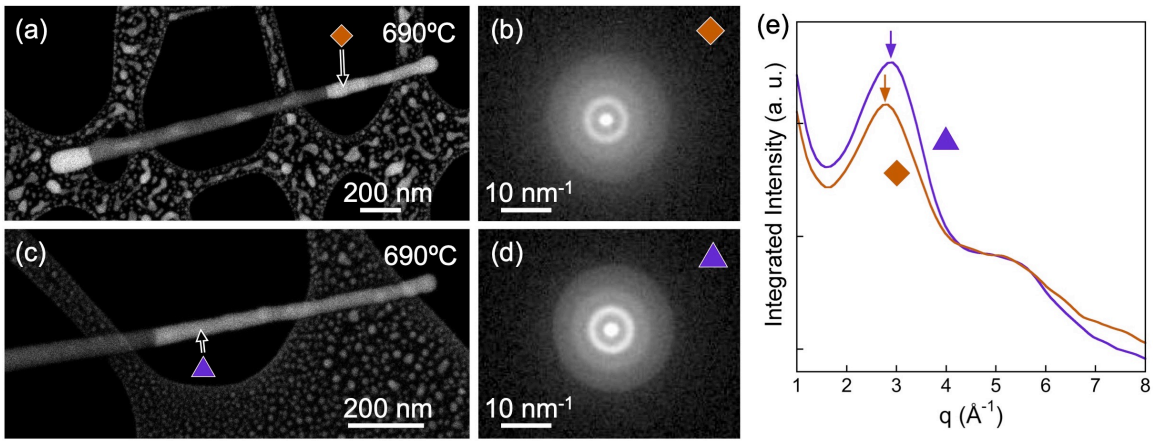

Figure S7. Comparison of nanobeam electron diffraction on AuGe melts in segments of thick and thin nanowires. (a) TEM image of a thick axially segmented nanowire (65 nm diameter) during annealing at 690°C. Liquid AuGe melt segments are imaged with bright contrast, whereas Ge segments appear dark. **(b)** High-temperature electron diffraction pattern (T = 690°C) from the AuGe melt segment, obtained at the position marked by an orange diamond in (a). **(c)** TEM image of a thick axially segmented nanowire (30 nm diameter) during annealing at 690°C. **(d)** High-temperature electron diffraction pattern (T = 690°C) from the AuGe melt segment, obtained at the position marked by a purple triangle in (c). **(e)** Radial distribution of the diffracted intensity of the liquid AuGe melts in thick (65 nm, diamond) and thin (30 nm, triangle) nanowires, showing the principal diffraction peak of the thinner wire shifted to larger spatial frequency (arrows), consistent with the results obtained on melt drops at the nanowire tips (Fig. 7 of the main text).